Applied Surface Science 394 (2017) 87–97

Contents lists available at ScienceDirect

Applied Surface Science

journal homepage: www.elsevier.com/locate/apsusc

Full Length Article

Structural and surface functionality changes in reticulated vitreous carbon produced from poly(furfuryl alcohol) with sodium hydroxide additions

Silvia Sizuka Oishi[a,*], Edson Cocchieri Botelho[b], Mirabel Cerqueira Rezende[c], Neidenêi Gomes Ferreira[a]

[a] LAS, Instituto Nacional de Pesquisas Espaciais (INPE), Av. dos Astronautas 1758, São José dos Campos, SP 12227-010, Brazil
[b] Departamento de Materiais e Tecnologia, Univ Estadual Paulista (UNESP), Av. Doutor Ariberto Pereira da Cunha 333, Guaratinguetá, SP 12516-410, Brazil
[c] Instituto de Ciência e Tecnologia, Universidade Federal de São Paulo (UNIFESP), Rua Talim 330, São José dos Campos, SP 12231-280, Brazil

ARTICLE INFO

Article history:
Received 2 August 2016
Received in revised form 14 October 2016
Accepted 17 October 2016
Available online 18 October 2016

Keywords:
Poly(furfuryl alcohol)
Reticulated vitreous carbon
Surface functionalities
Microstructure
NaOH oxidation

ABSTRACT

The use of sodium hydroxide to neutralize the acid catalyst increases the storage life of poly(furfuryl alcohol) (PFA) resin avoiding its continuous polymerization. In this work, a concentrated sodium hydroxide solution (NaOH) was added directly to the PFA resin in order to minimize the production of wastes generated when PFA is washed with diluted basic solution. Thus, different amounts of this concentrated basic solution were added to the resin up to reaching pH values of around 3, 5, 7, and 9. From these four types of modified PFA two sample sets of reticulated vitreous carbon (RVC) were processed and heat treated at two different temperatures (1000 and 1700 °C). A correlation among cross-link density of PFA and RVC morphology, structural ordering and surface functionalities was systematically studied using Fourier transform infrared spectroscopy, scanning electron microscopy, Raman spectroscopy, X-ray diffraction, and X-ray photoelectron spectroscopy techniques. The PFA neutralization (pH 7) led to its higher polymerization degree, promoting a crystallinity decrease on RVC treated at 1000 °C as well as its highest percentages of carboxylic groups on surface. A NaOH excess (pH 9) substantially increased the RVC oxygen content, but its crystallinity remained similar to those for samples from pH 3 and 5 treated at 1000 °C, probably due to the reduced presence of carboxylic group and the lower polymerization degree of its cured resin. Samples with pH 3 and 5 heat treated at 1000 and 1700 °C can be considered the most ordered which indicated that small quantities of NaOH may be advantageous to minimize continuous polymerization of PFA resin increasing its storage life and improving RVC microstructure.

1. Introduction

The preparation of carbon materials using poly(furfuryl alcohol) (PFA) has been extensively explored in many research papers [1–3]. With a growing concern about using materials obtained from renewable resources of low cost and accessibility, furan oligomers are an alternative to obtain polymers that present broad industrial application. Thus, furfuryl alcohol is the most important furan monomer used as precursor to different resin types [4,5] and carbon materials such as nanostructured carbons and nanocomposites [6–9], micro and nanoporous carbon [10–14], glassy carbon [3,15–17], among others. PFA can be obtained from a polycondensation reaction of furfuryl alcohol catalyzed by acids. Due to the furan ring great reactivity, curing and carbonization speed of furan resins are always faster compared to those of aromatic rings [18]. To avoid a violent reaction, the synthesis of PFA resin is carried out at low temperature (from 0 to 25 °C) and reaction time of up to 24 h [19–22]. The synthesis reaction can be finalized by cooling and neutralization to obtain the appropriate viscosity for the chosen application. In order to neutralize the acid catalyst, a solution of sodium hydroxide may be used to avoid continuous polymerization of PFA, increasing its storage life [20,22]. Some authors report that the neutralization process is slow and the PFA resin is usually washed several times with a diluted basic solution to avoid the emulsification [19,20]. However, this process generates toxic wastes due to the presence of monomers and PFA chains with low molecular weight. As a novelty of this work, it is proposed the neutralization of PFA with a minimum amount

* Corresponding author.
E-mail address: silviaoishi@uol.com.br (S.S. Oishi).

http://dx.doi.org/10.1016/j.apsusc.2016.10.112
0169-4332/

of concentrated NaOH solution which would avoid waste production. Also, the influence of this base on the crystalline structure and surface functionalities on vitreous carbon processed from this PFA must be investigated.

Vitreous carbon (or glassy carbon) is a form of carbon produced by the pyrolysis of an aromatic polymer, generally a phenolic or a PFA resin [16,23]. Reticulated vitreous carbon (RVC) is a porous foam-like structure and one of the most commonly carbon material used as electrode due mainly to the presence of many accessible pores with controlled sizes and high surface area, in addition to several other characteristics such as high chemical and thermal stabilities, catalytic properties, light weight, and low cost [2,23–27]. Normally, metals and alkali metals are added to non-graphitizing carbons in order to promote catalytic graphitization upon annealing [14,28–31]. The presence of sodium hydroxide can be evaluated as filler, which will affect the cross-link density of PFA and, consequently, the carbon properties and structural ordering processed from it. The carbon surface chemistry also influences many properties of carbon materials such as wetting, adsorption, catalysis, and electrochemical response [32–34]. As reported by Collins et al. [34], surface oxygen groups (SOG) are responsible for structure change, contributing to the partial graphitization process. However, SOG concentration in excess promotes graphite-like disorder. The structural influence of surface functionalities is rarely correlated with Raman or XRD. In this sense, the connection between Raman, XRD and surface functionalities results as well as among carbon material processing parameters is necessary for a complete understanding of their crystallite dimensions, graphitic-order, reactivity, and the structural influence of edge-site composition [34].

In this work the PFA resin acid catalyst was neutralized by adding different amounts of concentrated NaOH solution. Thus, our objective was to evaluate how this basic solution addition, which influences the cross-link density of cured PFA, can affect the processed RVC morphology, microstructure, and surface functionalities. To our knowledge, there are no papers in the literature that have tried to neutralize the PFA resin with a concentrated solution of NaOH and have showed a relationship between NaOH proportion in the PFA and the properties of processed carbon material. RVC was prepared using PFA resin with different amounts of concentrated sodium hydroxide solution until reaching pH of around 3, 5, 7 and 9. These samples were cured and subsequently submitted to heat treatment temperature (HTT) of 1000 and 1700 °C in order to obtain two sample sets with different graphitization indexes as a function of the PFA pH. All samples were characterized by Fourier transform infrared spectroscopy (FTIR), X-ray photoelectron spectroscopy (XPS), Raman spectroscopy, XRD, and scanning electron microscopy (SEM).

2. Experimental

2.1. Poly(furfuryl alcohol) with different sodium hydroxide amounts

PFA was synthesized according to the previously described procedure [35], using furfuryl alcohol (Fluka) and diluted sulfuric acid solution (Fmaia) (0.5 mol L^{-1}) as catalyst. The acid PFA resin (pH ~ 3) obtained after partial polymerization was distilled in a rotary evaporator at a reduced pressure until reaching moisture below 2 wt%. The resin was then separated in four portions to prepare resins with different pH values (pH 3, 5, 7 and 9). The pH of the resin was varied by adding a concentrated solution of sodium hydroxide (2.0 mol L^{-1}) until reaching the desired values without occurs emulsification. The resin pH control was accomplished by directly measuring the resin with a pH meter from Methrom 827 pH Lab, with a glass pH combination electrode (Unitrode). PFA viscosity varied from 12.9 Pas (pH 9 resin) to 21.0 Pas (pH 3 resin) at 25 °C. These measurements were performed in a Brookfield viscometer, model RV DV-II + Pro, with a SC4-34 spindle, using a shear rate of 8 s^{-1}, torque at 60.3% for pH 9 resin and shear rate of 6 s^{-1}, torque at 65.6% for pH 3 resin.

2.2. Reticulated vitreous carbon processing

Polyurethane foams with 70 pores per inch (ppi) were kindly donated by Sanko Espumas. The foams were cut into dimensions of 18 cm x 8 cm, followed by impregnation of about 20 g of PFA resins containing different quantities of sodium hydroxide. The resin was catalyzed with 3 w/w% of diluted *p*-toluenesulfonic acid (60 w/v%). Impregnated foams were cured in an oven for 1 h in the following temperatures: 50, 70, 90, 110, 130 °C. HTT of 1000 °C was carried out in a tube furnace from room temperature at heating rate of 1 °C/min in N_2 atmosphere reaching the maximum for 1 h up to its cooling down to room temperature. HTT of 1700 °C was carried out in similar way, except for using a heating rate of 5 °C/min. Characterizations are included in the Supplementary material.

3. Results

3.1. FTIR analysis

Fig. 1a shows the cured PFA FTIR spectra with different sodium hydroxide amounts. The band at 3400 cm^{-1} increased as a function of NaOH amount increase related to OH stretching [36]. Other characteristic bands of PFA are [19,37–40]: the bands at 2920 and 1430 cm^{-1} related to the aliphatic segments presence; the band at 1715 cm^{-1} due to the occurrence of some ring opening of furan ring; the band at 1560 cm^{-1} assigned to conjugated C=C species; the bands at 1506, 1157 and 1010 cm^{-1} attributed to furan ring; the band at 1360 cm^{-1} due to C—C or CO stretching; the band at 1220 cm^{-1} related to C—O from the alcohol or C—O—C of furan ring; and the band at 780 cm^{-1} characteristic of 2,5-disubstituted furan ring. The reaction progress (α) can be evaluated by the quotient among integrated intensity of primitive bands, i.e., $\alpha = I_{736} + I_{750}/(I_{782} + I_{790} + I_{803})$ [40]. The smaller this quotient, the farther the reaction has progressed. The decomposed bands at 736, 751, 782, 790, and 803 cm^{-1} were determined by spectra deconvolution in the interval from 700 to 850 cm^{-1} (Fig. 1b), using Gaussian shaped bands for the spectrum in absorbance. The calculated α values for pH 3, 5, 7, and 9 are 0.82, 0.79, 0.72, and 0.86, respectively. From these results, it can be inferred that sample pH7 presented the highest polymerization degree, since it had the lowest α value, followed by sample pH 5, 3 and 9 in descending order of polymerization degree.

3.2. Morphological and surface characterizations

RVC obtained from PFA resin with different NaOH additions for HTT at 1000 and 1700 °C were characterized by FEG-SEM images of their stems surfaces in two different magnifications (2000x and 10000×). Fig. 2 shows representative micrographs of RVC in which the nomenclature was created concerning the adjusted pH for each resin followed by its related RVC HTT values. RVC images heat treated at 1000 °C (RVC1000), indicate that pH3_1000 sample present a uniform texture resulted from good polyurethane foam impregnations. Sample pH5_1000 present a similar texture but at higher magnification it is possible to notice some irregular surface. On the other hand, pH7_1000 and pH9_1000 present morphologies significantly modified with higher roughness, attributed to the higher inclusions of sodium hydroxide. Some regions with agglomerates of NaOH and small pores can be seen in pH7_1000 sample and small crystals are visible over the whole pH9_1000 surface.

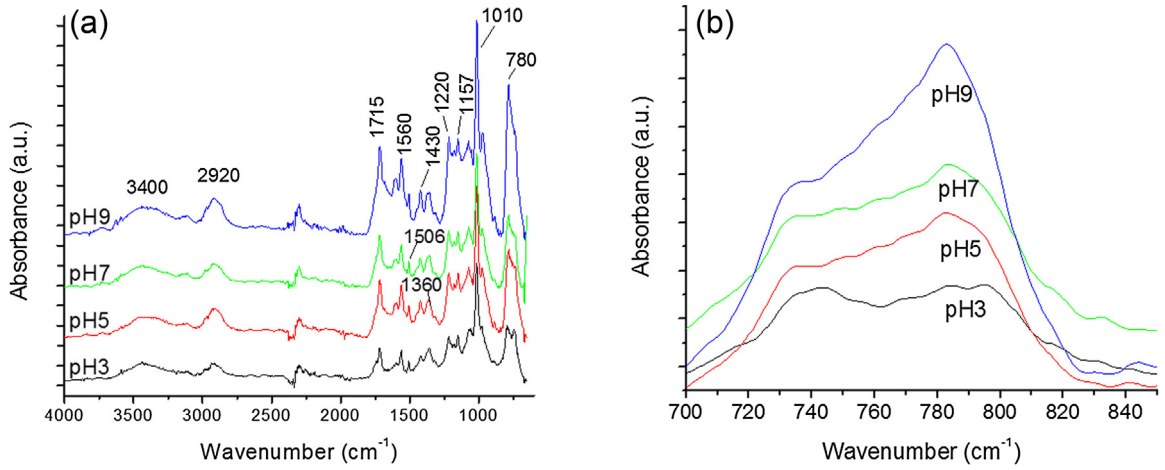

Fig. 1. FTIR spectra of cured PFA: a) FTIR spectra in absorbance ranging from 4000–600 cm^{-1}; b) FTIR spectra in absorbance in the interval 700–850 cm^{-1} used for the determination of α value for different pHs.

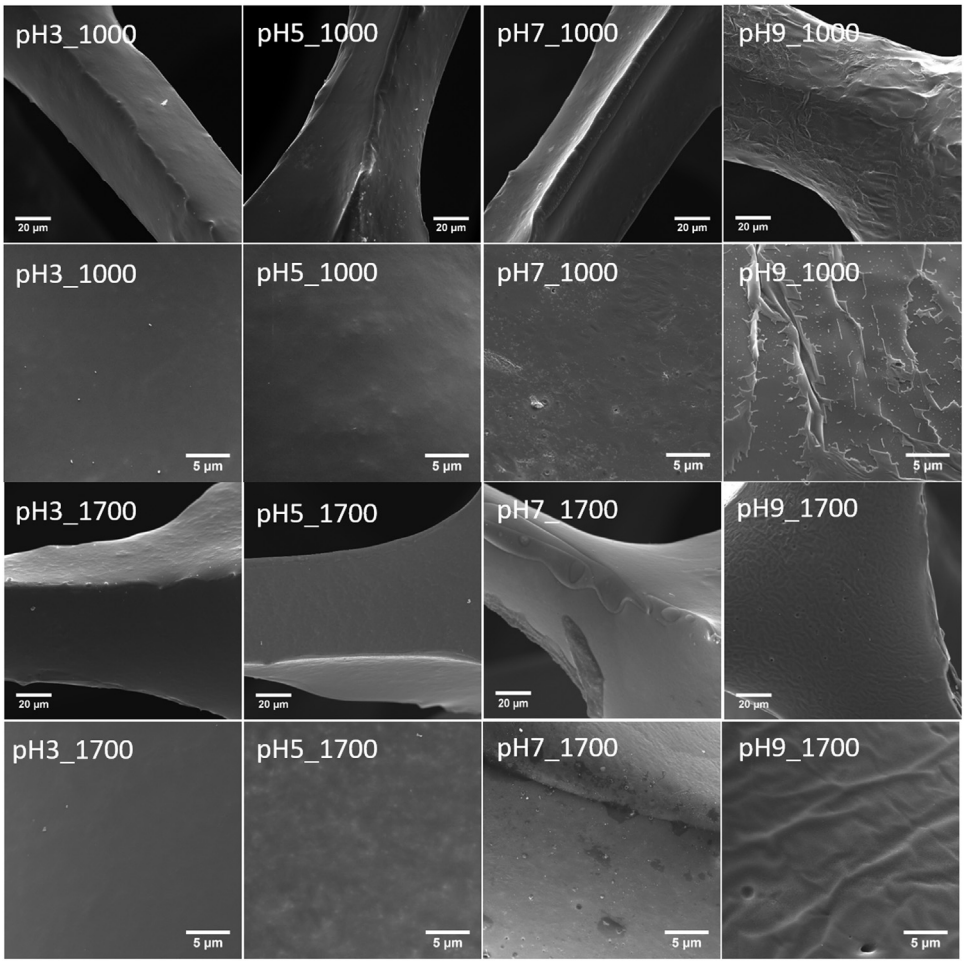

Fig. 2. FEG-SEM images of RVC1000 and RVC1700 samples in two different magnifications (2000× and 10000×).

The morphology of pH3_1700 and pH5_1700 samples remains visibly unchanged. However, small grains and/or pores with diameter around 0.7 μm are noted in the sample pH7_1700 attributed to NaOH removal. Furthermore, for sample pH9_1700, which presents the highest NaOH amount, the sodium hydroxide crystals seem to be completely volatilized leaving pores in the RVC matrix with very rough surface.

The presence of sodium compounds were confirmed by XPS analyses, which provide quantitative information of the sample surface compositions. The carbon, oxygen, and sodium atomic percentage, which are the possible elements found in the analyzed samples, are presented in Table 1. The O1s/C1s ratio, which indicates the degree of surface oxidation, is also included.

Table 1
Atomic percentage of carbon, oxygen and sodium and the O1s/C1s ratio of RVC1000 and RVC1700 samples processed from PFA with different pH values adjusted with sodium hydroxide.

Composition (atomic%)				
Sample	C1s	O1s	Na1s	O1s/C1s ratio (%)
pH3_1000	95.37	4.65	–	4.88
pH5_1000	93.59	6.41	–	6.85
pH7_1000	92.04	7.85	0.10	8.53
pH9_1000	74.00	21.45	4.55	28.99
pH3_1700	97.84	2.16	–	2.21
pH5_1700	98.81	1.19	–	1.20
pH7_1700	98.18	1.82	–	1.85
pH9_1700	98.60	1.40	–	1.42

The NaOH addition increase on PFA tends to decrease the carbon amount on the respective processed RVC1000 samples, which is associated to their oxygen concentration increase. Thus, the O1s/C1s ratio reflects exactly the expected behavior. Sodium could be identified only on samples pH7_1000 and pH9_1000. For 1700 °C HTT, the carbon concentration increases for all samples, while the oxygen loss occurs and the sodium compounds disappear. These results confirm that the volatilization of sodium compounds generate a rough surface.

Fig. 3 shows high-resolution XPS spectra and the curve fitting of C1s region for samples pH3 and 9 at 1000 and 1700 °C. The peak position and FWHM (full width at half maximum) constraints for the curve fitting were assigned according to the literature [41–45]. Six peaks were considered: graphitic (~284.4 eV, peak I), β-carbon (~285.2 eV, peak II), hydroxide or ether (~286.1 eV, peak III), carbonyl (~287.7 eV, peak IV), carboxyl or ester (~288.8 eV, peak V) and π-π* shake-up (~290.6 eV, peak VI). Some authors correlate the 290.6 eV position to CO, CO_2 and carbonate groups [45,46] or also as aromatic structure [47,48]. The percentages of each functional group determined by XPS for RVC1000 and 1700 with different pHs are shown in Fig. 4. There is a decrease in the relative content of graphitic carbon (C—C) with NaOH addition, mainly for samples pH7_1000 and pH9_1000. For these samples the peak related to C—OH decreases, whereas an increase occurs mostly in the peak assigned to a second graphitic peak (carbons bonded to oxidized carbons) [41,44] and C=O, respectively. This fact shows that NaOH acts as an oxidant, increasing the degree of oxidation for samples pH7_1000 and pH9_1000, where the carbon components bonded with oxygen are more pronounced in C1s spectrum when compared to those for pH3_1000. Sample ph9_1000 exhibits a prominent bump at 290.6 eV, related to π-π* shake-up, which is probably induced by the NaOH excess.

For RVC treated at 1700 °C, FWHM of C1s spectra (Fig. 3b and d) visually decreases due to the oxidize carbon components decrease. The removal of some surface functionalities is expected as it can be observed by the C—OH, C=O and COOH groups decrease and by an increase of C—C and β-carbon for sample pH3 and pH5. However, samples pH7_1700 and pH9_1700 showed an increase in C—OH coming from a more oxidative state similarly to those for samples pH7_1000 and pH9_1000. In addition, sample pH9_1700 present an increase in COOH group due to a decrease in the peak related to π-π* shake-up, while samples in other pH values at this HTT presented a decrease in COOH group.

Fig. 5 shows the O1s spectra fitted for both samples pH 3 and 9 heat treated at 1000 and 1700 °C. For the curve fitting of O1s spectra, four dominant components of oxidized carbon were considered [49,50], named C=O at ~531.1 eV (peak I); hydroxyls, ethers and C=O in esters, amides, anhydrides at 532.3 eV (peak II); C—O in esters and anhydrides at 533.3 eV (peak III); carboxylic groups at 534.2 eV (peak IV); and adsorbed water at 536.0 eV (peak V). For sample pH9_1000 (Fig. 5c), the presence of sodium hydroxide at ~532.8 eV was considered. Fig. 6 presents the percentage of surface oxygen functional group. The content of oxygen atoms of peak I for RVC1000 samples varies from 10.2% (pH5_1000) to 17.4% (pH9_1000) while for RVC1700 samples, peak I decreases with percentages from 4.0% (pH5_1700) to 7.92% (pH7_1700). Peak II is predominant in relation to the other peaks for both RVC1000 and 1700 samples with the exception of pH3_1000, pH9_1000 and pH7_1700 samples that present values of 40.4, 19.8 and 31.7%, respectively. These same set of samples pH3_1000, pH9_1000 and pH7_1700 show the largest percentage of peak III in relation to the other components, with values of 40.8, 29.1, and 39.6%, respectively. For peak IV, the percentages from 2.75% (pH9_1000) to 20.0% (pH7_1000) were obtained. However, for RVC1700 samples, peak IV increases varying from 11.7% (pH5_1700) to 24.9% (pH9_1700). The oxygen atoms from NaOH appeared only on sample pH9_1000 and were estimated at 16.2%. In addition, this sample also presented a prominent band at 536 eV, which is probably related to Na KLL and not to adsorbed water.

3.3. XRD analysis

Carbon materials quality is usually assessed by X-ray diffraction (XRD) and Raman spectroscopy. Both techniques are complementary and can provide information about the carbon crystallinity. The determination of carbon crystallinity by XRD has been well established with good reproducibility [51–53]. XRD may provide information from the bulk due to its penetration depth of around 500 μm in carbon material [54], while Raman spectroscopy has as advantage a higher surface selectivity thus providing less averaged information with an estimated sampling depth of about 100 nm [16,53]. Fig. 7 presents the diffraction patterns of RVC1000 and RVC1700 for all pH variations. The investigated RVC samples show carbon bands at 2θ around 24.5°, 43.6° and 80.0° for RVC1000 and 24.8°, 43.5° and 79° for RVC1700. These bands correspond to the reflections (002), (10) and (11), respectively. Comparing RVC1000 and 1700 XRD patterns, all the bands show an intensity and narrowing increase after 1700 °C HTT, indicating an improvement of graphitization index. Comparing the pH variations, the highest change in intensity and width occurs for (002) band that is related to the graphitic stacking structure, while small variation occurs for (10) band which is associated with the in-plane structure. Fig. 8 shows the effects of pH and HTT for the interlayer spacing (d_{002}), crystallite height (Lc), and crystallite width (La). The interlayer spacing (Fig. 8a) of RVC1000 is of about 0.366 nm for samples pH3, pH5 and pH7 showing slight increase for pH9_1000 of 0.367 nm, which may be associated to defects on graphitic sheets due to the NaOH contribution. For RVC treated at 1700 °C, there is a modest decrease in d_{002} for all samples in comparison to those of RVC1000 and one can highlight pH5_1700 sample as the highest interlayer ordering. Analyzing Lc values, pH5_1000 and pH5_1700 samples exhibit the highest crystallite height among samples with different pH in both HTT. A discrete variation occurs among La values of samples with different pHs for both set of samples (RVC1000 and RVC1700). One can also highlight samples pH7 heat treated at 1000 and 1700 °C, which present the lowest crystallite width.

3.4. Raman spectroscopy results

Raman spectroscopy results were discussed in order to evaluate the possible structural changes with sodium hydroxide addition at different RVC HTT. The D band (~1350 cm^{-1}) represents disordered structure of carbon and reflects sp^2 vibration of the rings, which is caused by defects such as impurities, edges and finite-size effects that destruct the translational symmetry of A_{1g}. D-band intensity is proportional to the presence of six fold aromatic rings. The G band, on the other hand, corresponds to graphite in-plane vibrations with

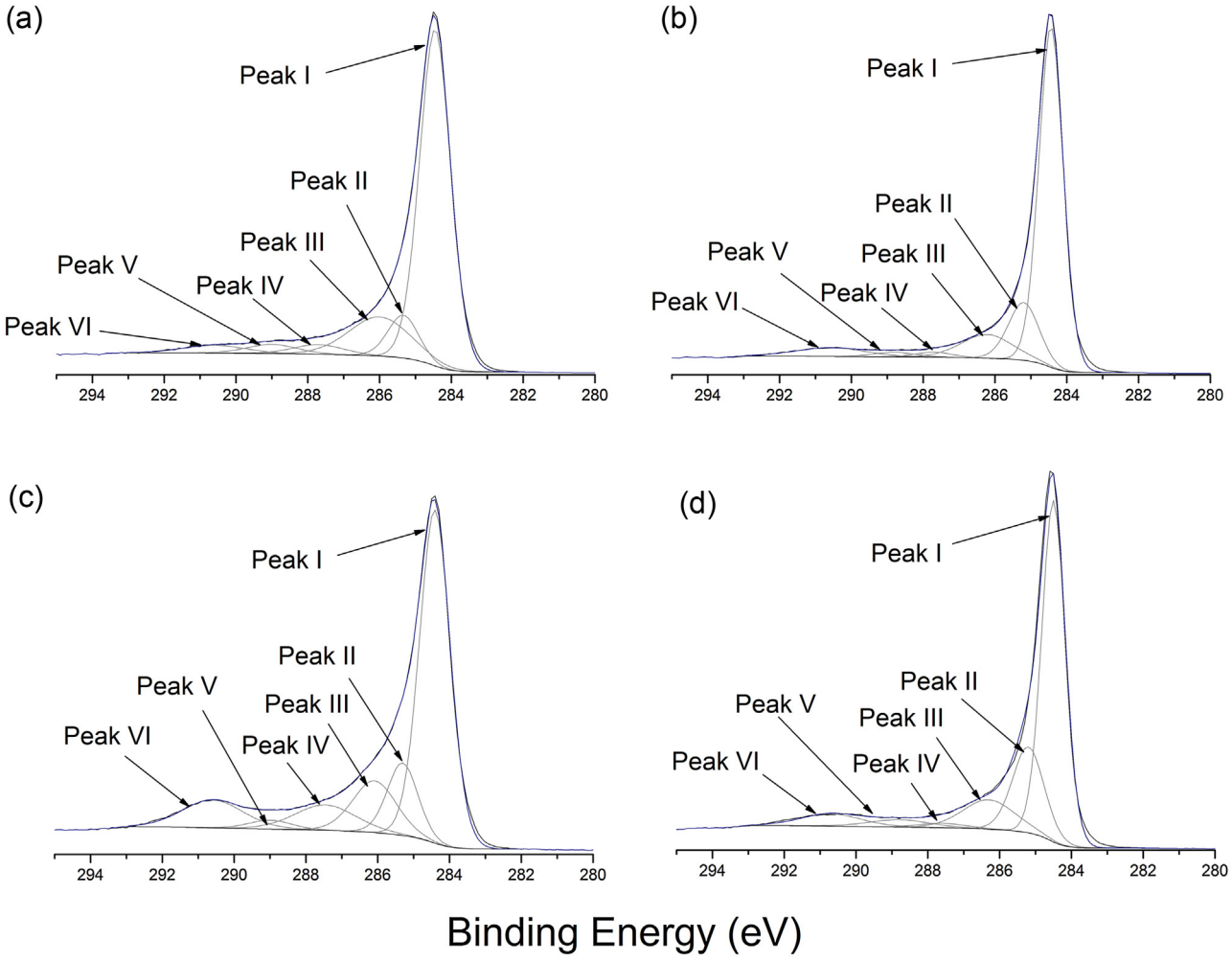

Fig. 3. Curve fitting of C1s spectra of: a) pH3_1000; b) pH3_1700; c) pH9_1000; and d) pH9_1700.

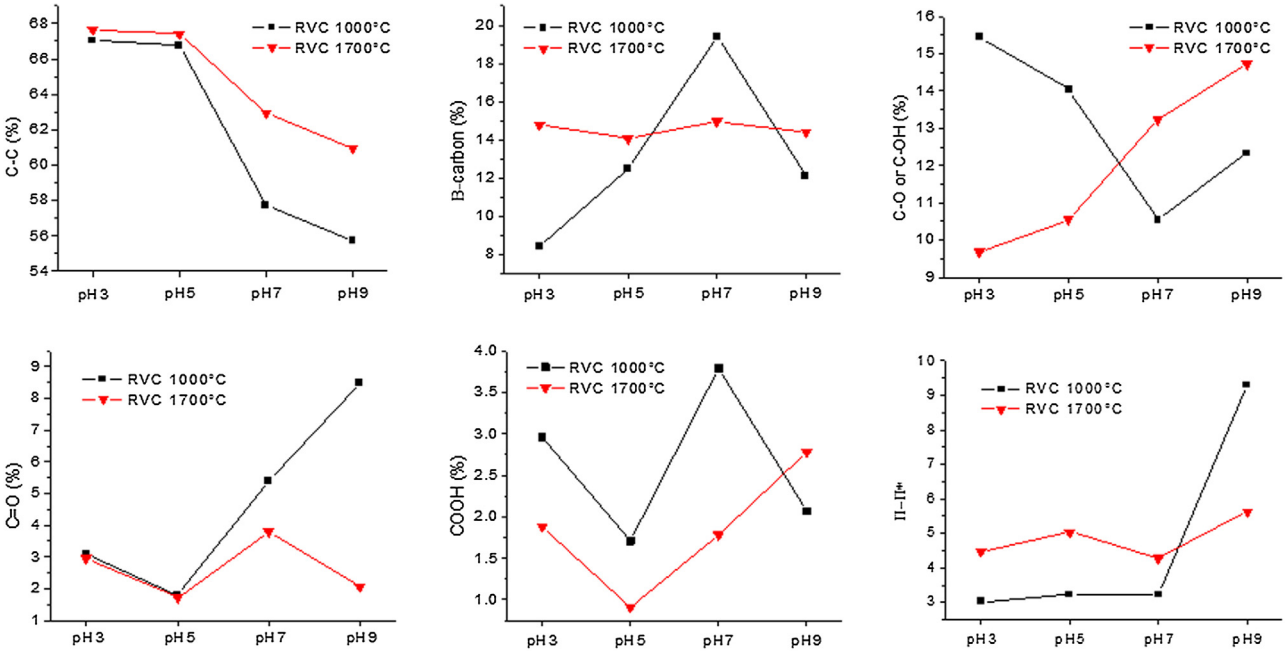

Fig. 4. Percentages of each surface functional group from C1s spectra for RVC1000 and 1700 with different pH values.

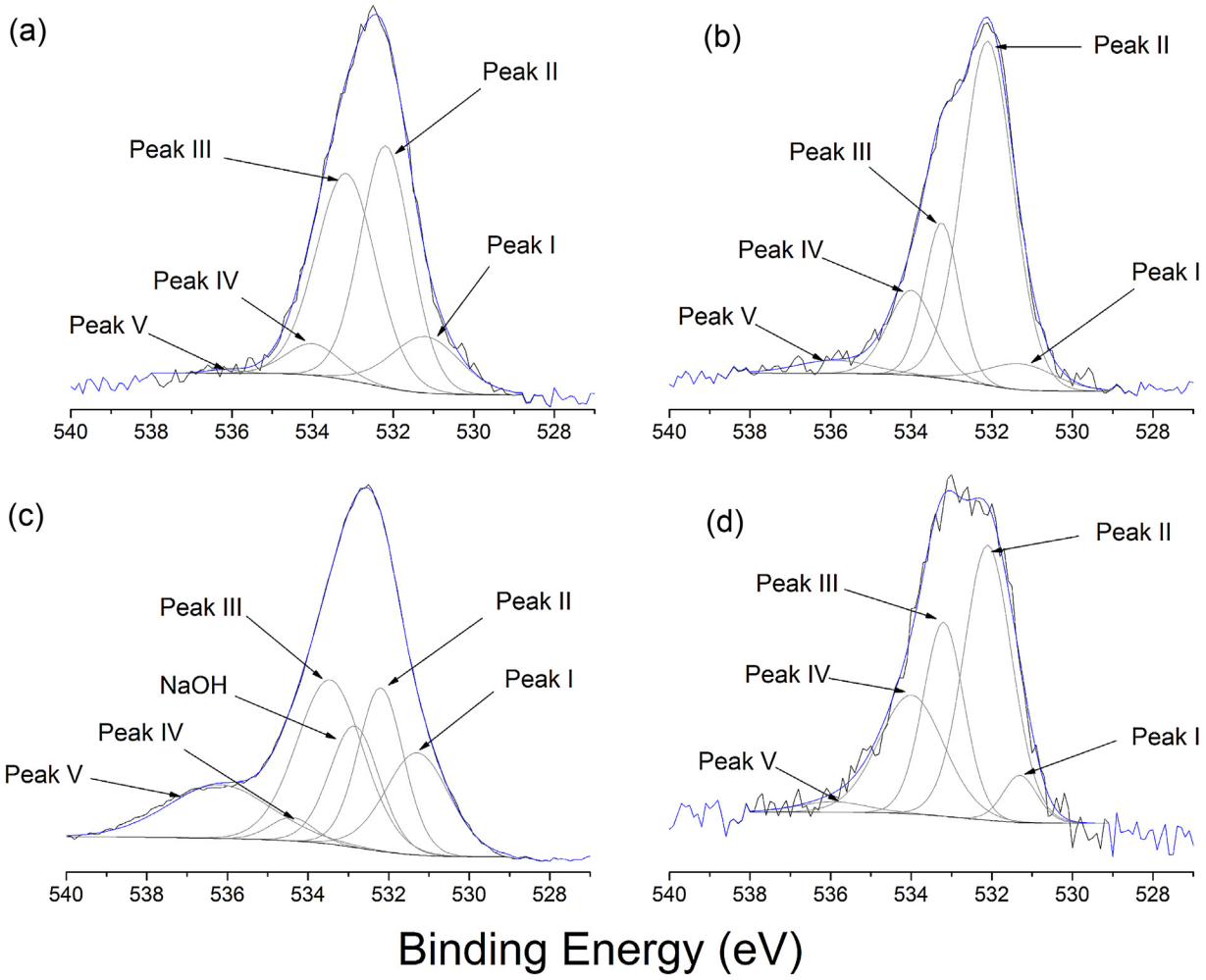

Fig. 5. Curve fitting of O1s spectra of: a) pH3_1000; b) pH3_1700; c) pH9_1000; and d) pH9_1700.

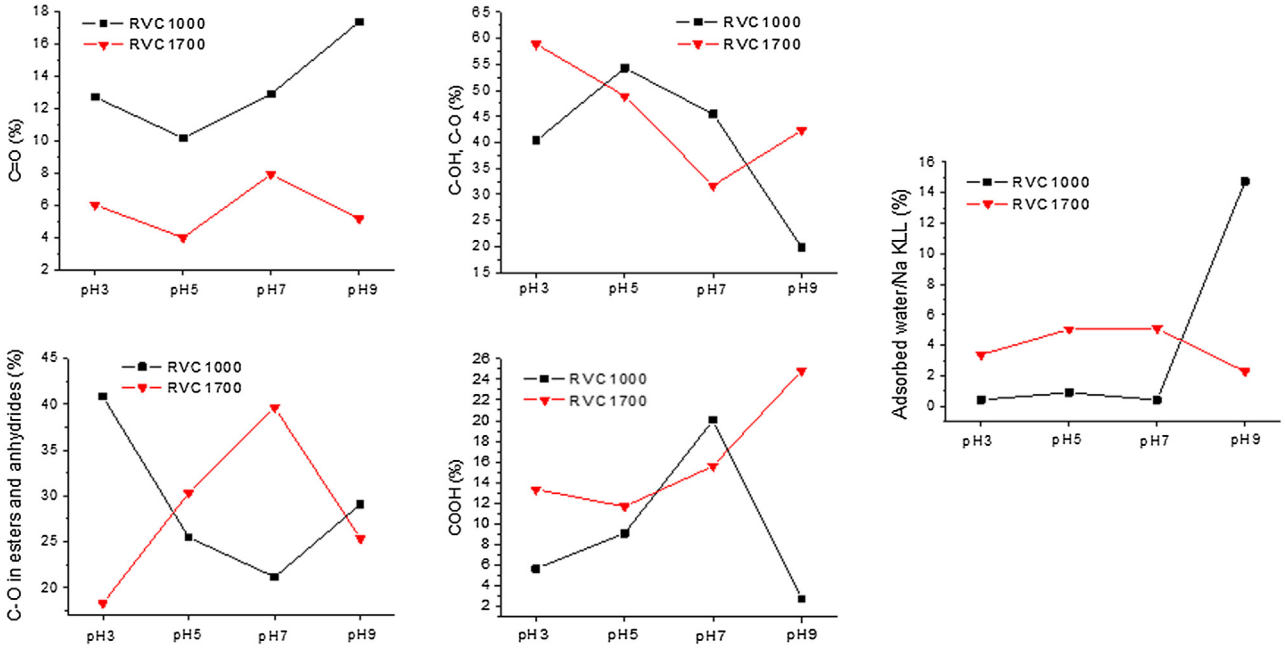

Fig. 6. Percentages of each surface functional groups from C1s spectra for RVC1000 and 1700 with different pHs.

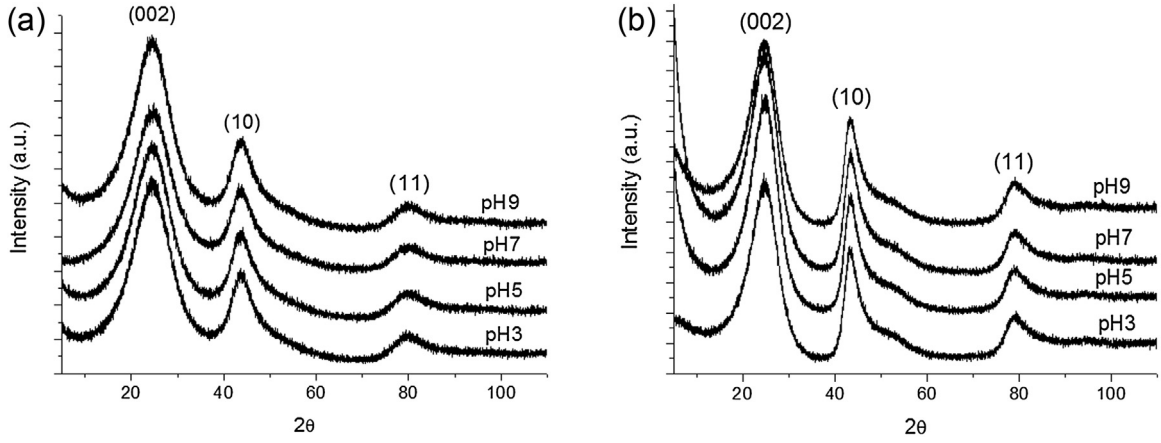

Fig. 7. X-ray diffractograms of: a) RVC1000 and b) RVC1700 for all pH variations.

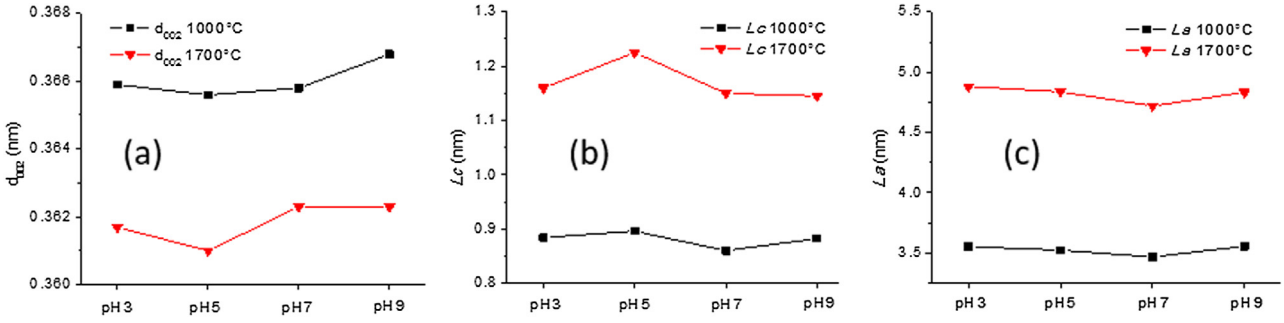

Fig. 8. Interlayer spacing, d_{002} (a), crystallite height, Lc (b), and crystallite width, La (c), derived from Bragg and Scherrer equations.

E_{2g} symmetry which reflects the degree of graphitization. G-band intensity is proportional to the presence of any sp^2 bonds, not only to those in the rings [55–57].

The G band in glassy carbon is presented as a superposition of the G and D' (~1620 cm^{-1}) bands [16]. The D' band also corresponds to E_{2g} symmetry of graphitic structure. A band between 1165 and 1200 cm^{-1}, named I, is assigned to disordered structures formed from the original polymeric structure, polyenes and ionic impurities [58,59]. Another first-order band, denominated D", is located at ~1500 cm^{-1} and is related to sp^2 amorphous carbon band [58,59].

Fig. 9 presents the first and second order Raman spectra of RVC1000 and 1700 with different pH values. The Raman spectra of carbonaceous materials have been continuously studied and new visions and interpretations have been published recently in the literature [13,60,61]. In this work, the analyses and determination of spectral parameters by curve fitting were based on the best bands combination as presented by Sadezky et al. [59], i.e., Lorentzian-shaped bands G, D, D', and I bands (1580, 1350, 1620, and 1200 cm^{-1}, respectively), and Gaussian-shaped D" band (~1500 cm^{-1}). The D and G band parameters like full width at half maximum (FWHM) and intensity ratio of D and G bands (I_D/I_G), are useful to estimate the degree of ordering in carbonaceous materials. In case of low crystallinity samples, the use of second order bands is a solution when I_D/I_G ratio shows a conflicting behavior, but only if the second order is clear enough to be analyzed [60]. Therefore, the second order bands were fitted only for RVC1700 samples due to the broad bands of RVC1000 samples. Four Lorentzian-shaped bands with their initial positions at 2450, 2700, 2900, and 3100 cm^{-1} (named 2I, G', D+G, and 2D', respectively) were used according to Sadezky et al. [59]. The D, G and G' are the three main bands of graphite and their intensity ratios combinations and FWHM are shown in Fig. 10.

I_D/I_G ratio is associated with in-plane defects, such as point defects, dislocations and finite size boundaries [62]. Thus, I_D/I_G ratio decreases as sample disorder decreases. Several works have demonstrated the PFA behavior when subjected to heat treatment at different temperatures [13,54,63–67]. In this work, comparing I_D/I_G ratio for samples heat treated at 1000 and 1700 °C (Fig. 10a), I_D/I_G ratio decreases after 1700 °C HTT, as expected due mainly to an increase in the sample graphitization degree. For RVC1000, pH7 sample presents the highest disorder and there are no significant changes among the samples with other pH values. For RVC1700, pH 5 presents I_D/I_G ratio slightly lower than other samples.

The narrowing of D and G band widths are related to the release of heteroatoms from the polymeric precursor and is also associated to the decrease of structural defects [54]. A decline for both D and G band after 1700 °C HTT is evident from FWHM of D and G bands (wD and wG, respectively) in Fig. 10b and c, due to the oxygen release. An increase in wD and wG values as a function of pH increase for RVC1000 samples is expected since the sodium hydroxide addition increases the oxygen concentration in the matrix, as already previously shown by XPS analyses. However, among samples with different pH values of RVC1000 and 1700 there is a slightly difference at wD and wG and no trend is observed.

For samples with short La (between 2 and 3 nm), the second order band intensity ratios display a clear behavior [60]. For example, an increase in $I_{G'}/I_G$ is associated with an increase in crystallinity, while $I_D/I_{G'}$ increase is assigned to a decrease in crystallinity [60]. From the analyses of $I_{G'}/I_G$ and $I_D/I_{G'}$ ratios (Fig. 10d and e) for RVC1700, the differences among different pH samples become more evident, i.e., pH 3 sample can be highlighted as the most ordered sample while pH 7 as the most disordered. The G' is sensitive to structure changes and wG' must decrease as the crystallinity increase [51]. According to Antunes et al. [68], wG' is of

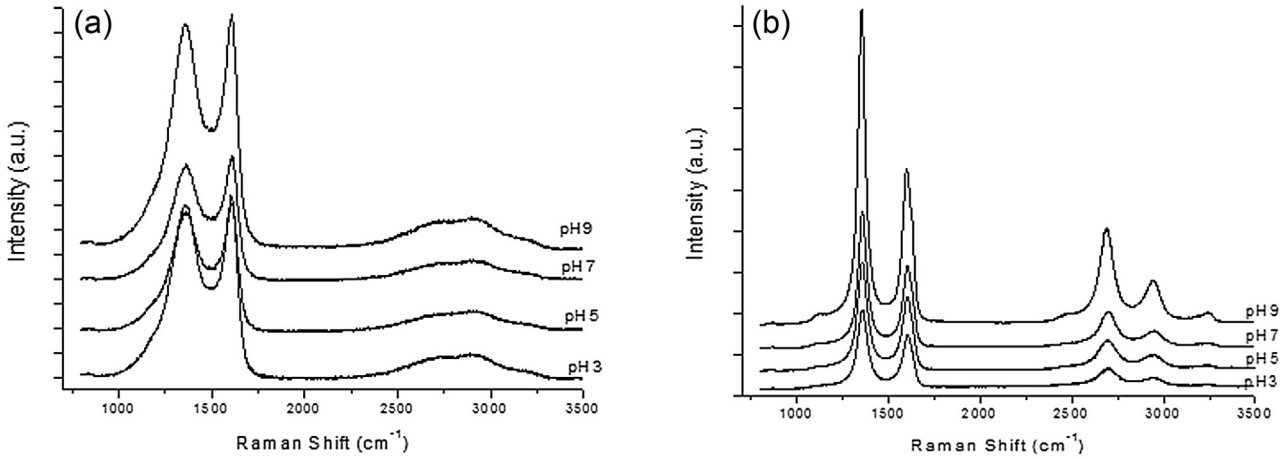

Fig. 9. Raman spectra of: a) RVC1000 and b) RVC1700 processed from PFA with different pH variations.

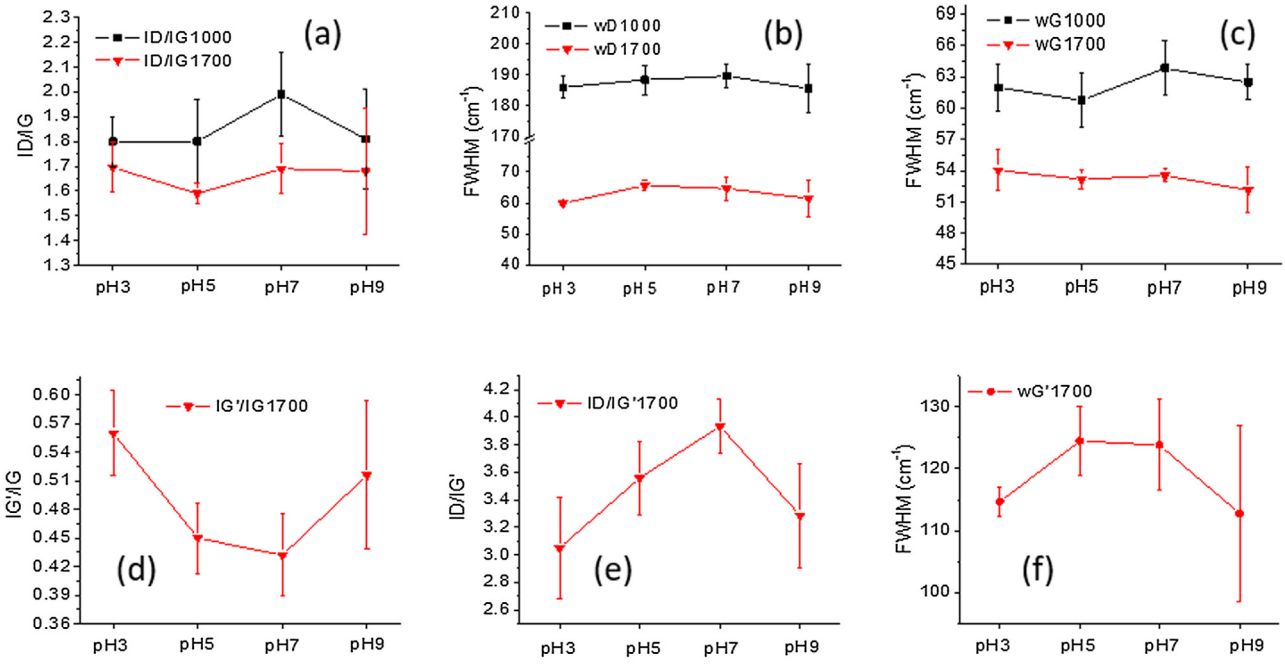

Fig. 10. Graphics of: a) ID/IG ratio, b) wD, c) wG, d) IG'/IG ratio, e) ID/IG' ratio and f) wG' for RVC1000 and/or RVC1700 with different pH values.

about twice wG and should exhibit the same trend. For this work, wG' shows a different trend of wG, which can be related to inaccuracy in the G band fitting. Therefore, in case of uncertainty in the G band fitting, the $I_D/I_{G'}$ ratio is a more reliable alternative [60].

A higher standard deviation can be observed for both samples pH9_1000 and pH9_1700 that can be assigned to their higher heterogeneity caused by the excess of NaOH addition. Barros et al. [62,69] noted that in the case of graphitic foams, both 2D and 3D graphite regions were found due to the foam three-dimensional geometry that present spherical cells intersecting with each other, forming pores and junctions between them. The region of the junction, where the ligaments meet, have shown the presence of highly curved and folded graphitic planes [69]. Moreover, the region of curvature of cell walls also naturally originates 2D graphite regions. Therefore, the anisotropic nature of RVC foams also justifies the dispersion of intensity ratios and FWHM standard deviation for all samples.

The crystallite size were also estimated by Raman spectra using the general equation proposed by Cançado et al. [70], i.e., $La = \left(2.4x10^{-10}\right)\lambda_{laser}{}^{4}\left(\frac{I_D}{I_G}\right)^{-1}$, where I_D/I_G is the integrated intensity ratio of the D and G bands. Table 2 shows a comparison between La results obtained by Raman and XRD. The La calculated for samples with HTT at 1000 °C present approximated values for both Raman and XRD. On the other hand, samples with HTT at 1700 °C present higher La when estimated by Raman than those of XRD. Baldan et al. [54] has also observed this discrepancy at higher HTT that can be

Table 2
La values obtained by Raman and XRD.

Sample	La (nm) from Raman	La (nm) from XRD
pH3_1000	3.41	3.56
pH5_1000	3.32	3.52
pH7_1000	3.12	3.47
pH9_1000	3.44	3.56
pH3_1700	8.52	4.88
pH5_1700	8.35	4.84
pH7_1700	8.21	4.72
pH9_1700	8.56	4.83

mainly related to the use of the area ratio where the effect of line broadening is included in the calculation. However, it is important to note that La calculated by Raman has the same tendency and discrete variation in different pH values for both HTT when compared to La calculated by XRD. This fact indicates that the crystallinity of the bulk and the carbon surface are quite similar. According to Arzani et al. [71], La can be considered an indicator for degree of functionalization on the surface and edges of graphene nanoparticles. Taking into account that the lower La value the higher is the density of defects on the surface due to the higher degree of functionalization [71], samples pH7_1000 and pH7_1700 present the higher density of defects. However, in this case, the higher density of defects is not only from the degree of functionalization but also probably from the presence of some specific functional groups, since sample pH9_1000 present the highest degree of functionalization with oxygen functional groups.

4. Discussion

Polymer modification may provide desired or undesired properties for the final carbon material. This research aimed at investigating how the NaOH addition used to neutralize the acid catalyst of PFA resin affected its degree of polymerization and, consequently, the processed RVC crystallinity, morphology, and surface functionalities. The sodium hydroxide addition seemed to increase the degree of polymerization of PFA resin up to pH 7 while it decreased for resin with pH 9 as shown by FTIR analyses. This result showed that only an excess of NaOH hinders the cross-link formation in PFA samples. For higher levels of cross-linking, the reorganization is difficult at high temperature, then a less ordered sample is expected. On the other hand, more ordering may occur at lower levels of cross-linking for the same HTT [72]. In this case, Raman results showed a good agreement for RVC1000 samples, i.e., pH7_1000 showed the highest disorder considering I_D/I_G ratio, wD, and wG while for the other RVC1000 samples I_D/I_G ratio and wD were quite close.

Carboxylic acid is one of oxygen-containing groups responsible to transform aromatic π-density into olefin π-density by breaking aromatic bonds resulting from the attachment of carboxylic group, which enables the extended conjugation of the carbon system increasing crystallite dimension (La) [73]. On the other hand, a high yield in carboxylic groups is associated with an intense aromatic ring cleavage and, consequently, a damage of aromatic sheets [48]. The NaOH oxidation effects were confirmed by XPS analyses, which showed an increase in surface oxidation degree with increasing the NaOH amount. An increase in oxygen content led to an increase in disorder mainly for pH7_1000 sample as shown by Raman analysis. In this case, the highest disorder of pH7_1000 can be related to its highest percentages of carboxylic acid verified in C1s and O1s spectra, besides the highest degree of polymerization in its related PFA resin. The largest content of oxygen (21.45%) was observed for pH9_1000 sample, which should be associated to its high level of defects. However, this sample presented a similar ordering as those for pH3_1000 and pH5_1000 samples considering I_D/I_G ratio and FWHM. The graphitic ordering of sample pH9_1000 is being influenced by the reduced presence of carboxylic group that is an indicative of lower damage of aromatic sheets and by the lowest degree of polymerization of its cured PFA resin. XRD analysis showed a d_{002} slightly higher for pH9_1000 sample, probably generated by stacking faults resulting from the presence of heteroatoms and also steric hindrance between surface functionalities.

The annealing under inert atmosphere until 1700 °C removed the NaOH and most of surface oxygen groups, increasing the carbon composition to approximated values (ranging from 98 to 99%, as shown in Table 1) among different pH values. The heteroatoms released increased the crystallinity leading to a better organization of graphene sheets comparing to RVC1000 samples, as shown by XRD and Raman analyses. For RVC1700 samples, the use of second order Raman bands was possible due to a more defined bands. Moreover, the variation among different pH was more evident on intensity ratio ($I_G/I_{G'}$ and $I_D/I_{G'}$) and FWHM of G' band (Fig. 10d–f) in comparison to the results of first order Raman bands that showed little variation (Fig. 10a–c). From the second order Raman G' band results, pH7_1700 sample continued presenting the highest disorder as well as pH7_1000 sample, probably due to the predominant effect of higher degree of polymerization of its cured PFA resin which hinders the structure reorganization. A good structural organization of pH3_1700 sample was expected owing to the purity of its precursor resin. On the other hand, sample pH9_1700 has presented the average values of intensity ratio ($I_{G'}/I_G$ and $I_D/I_{G'}$) and FWHM (wG') close to those of pH3_1700, but it also presented a high standard deviation. The higher standard deviation of pH9_1700 sample may be derived from some regions with higher defects that are concentrated in the unaligned regions of the material confirmed by the strong D-band in Fig. 9b, as reported by Barros et al. [69]. Besides, the damage of aromatic sheets can be confirmed by an increase in carboxylic groups (Figs. 4 and 6) of pH9_1700 compared to other RVC1700 samples. Some regions with increased graphitic ordering on pH9_1700 sample may have resulted from the high oxygen content (around 21%) observed on pH9_1000 sample that was removed with the smallest graphitic crystallites during heat treatment at 1700 °C leaving the larger crystallites, as well as may have consumed the disordered carbon increasing the degree of organization of pH9_1700 sample.

Considering XRD results (d_{002}, Lc, and La), pH5_1000 and pH5_1700 samples presented the best graphitic ordering, which was an indicative that little amount of NaOH can be beneficial to minimize continuous polymerization of PFA resin and improve RVC microstructure of carbon bulk.

5. Conclusions

FTIR analyses showed that cured PFA resin with pH 7 presented the highest degree of polymerization while the lowest was observed for pH 9 resin. This means that only an excess of NaOH reduced the cross-link formation. The O1s/C1s ratio obtained by XPS indicated that NaOH addition increased the oxygen concentration for RVC1000 samples, consequently, an increase in RVC disorder would be observed. However, sample pH9_1000, which presented the highest oxygen content, had a similar ordering to those for samples pH3_1000 and pH5_1000 when Raman parameters were analyzed. This behavior was attributed to the reduced presence of carboxylic group and also by its processing from PFA with the lowest degree of polymerization. On the other hand, sample pH7_1000 presented the highest disorder due to the highest carboxylic acid percentage among RVC1000 samples, associated to its processing from the cured PFA with the highest degree of polymerization. After 1700 °C HTT, the removal of oxygen and NaOH led the carbon composition to close values considering the different pH samples. Sample pH7_1700 showed the highest disorder probably due to the predominant effect of its cured PFA resin with the highest degree of polymerization. The most ordered sample was exhibited for pH3_1700. Although sample pH9_1700 showed the average values of I_D/I_G intensity ratio and FWHM close to those of pH3_1700, its high standard deviation demonstrated the presence of regions with high defect concentrations. XRD analyses, which provide information from the carbon bulk, showed samples pH5_1000 and pH5_1700 as the most ordered, which means that the addition of small quantities of NaOH in the PFA resin may be advantageous to minimize continuous polymerization of PFA resin

and improve RVC microstructure. In general, the structural ordering was mainly influenced by the predominant effect of the cured PFA polymerization degree and carboxylic acid content on RVC surface.

Acknowledgements

The authors acknowledge the financial support from grant #162683/2013-8 and 303287/2013-6 CNPq, grant #2014/27164-6 São Paulo Research Foundation (FAPESP) and CAPES/PVNS. Special thanks to Dr. M.R. Baldan by XPS measurements.

Appendix A. Supplementary data

Supplementary data associated with this article can be found, in the online version, at http://dx.doi.org/10.1016/j.apsusc.2016.10.112.

References

[1] B.A. Samuel, R. Rajagopalan, H.C. Foley, M.A. Haque, Effect of pyrolysis temperature on the microstructure of disordered carbon nanowires, Thin Solid Films 519 (2010) 91–95, http://dx.doi.org/10.1016/j.tsf.2010.07.066.
[2] N. Amini, K.F. Aguey-Zinsou, Z.X. Guo, Processing of strong and highly conductive carbon foams as electrode, Carbon N.Y. 49 (2011) 3857–3864, http://dx.doi.org/10.1016/j.carbon.2011.05.022.
[3] E. Cocchieri Botelho, N. Scherbakoff, M.C. Rezende, Porosity control in glassy carbon by rheological study of the furfuryl resin, Carbon N.Y. 39 (2001) 45–52, http://dx.doi.org/10.1016/S0008-6223(00)00080-4.
[4] A. Gandini, Furans as offspring of sugars and polysaccharides and progenitors of a family of remarkable polymers: a review of recent progress, Polym. Chem. 1 (2010) 245–251, http://dx.doi.org/10.1039/b9py00233b.
[5] A. Gandini, Polymers from renewable resources: A challenge for the future of macromolecular materials, Macromolecules 41 (2008) 9491–9504, http://dx.doi.org/10.1021/ma801735u.
[6] H. Wang, J. Yao, Use of Poly(furfuryl alcohol) in the fabrication of nanostructured carbons and nanocomposites, Ind. Eng. Chem. Res. 45 (2006) 6393–6404, http://dx.doi.org/10.1021/ie0602660.
[7] X.H. Men, Z.Z. Zhang, H.J. Song, K. Wang, W. Jiang, Functionalization of carbon nanotubes to improve the tribological properties of poly(furfuryl alcohol) composite coatings, Compos. Sci. Technol. 68 (2008) 1042–1049, http://dx.doi.org/10.1016/j.compscitech.2007.07.008.
[8] B. Yi, R. Rajagopalan, H.C. Foley, U.J. Kim, X. Liu, P.C. Eklund, U.V. Park, V. Pennsyl, Catalytic polymerization and facile grafting of poly (furfuryl alcohol) to single-wall carbon nanotube: preparation of nanocomposite carbon, J. Am. Chem. Soc. 128 (2006) 11307–11313, http://dx.doi.org/10.1021/ja063518x.
[9] L.A. Pranger, G.A. Nunnery, R. Tannenbaum, Mechanism of the nanoparticle-catalyzed polymerization of furfuryl alcohol and the thermal and mechanical properties of the resulting nanocomposites, Compos. Part B: Eng. 43 (2012) 1139–1146, http://dx.doi.org/10.1016/j.compositesb.2011.08.010.
[10] C. Song, T. Wang, H. Jiang, X. Wang, Y. Cao, J. Qiu, Gas separation performance of C/CMS membranes derived from poly(furfuryl alcohol) (PFA) with different chemical structure, J. Memb. Sci. 361 (2010) 22–27, http://dx.doi.org/10.1016/j.memsci.2010.06.018.
[11] J. Yao, H. Wang, J. Liu, K.Y. Chan, L. Zhang, N. Xu, Preparation of colloidal microporous carbon spheres from furfuryl alcohol, Carbon N. Y. 43 (2005) 1709–1715, http://dx.doi.org/10.1016/j.carbon.2005.02.014.
[12] C.L. Burket, R. Rajagopalan, H.C. Foley, Overcoming the barrier to graphitization in a polymer-derived nanoporous carbon, Carbon N. Y. 46 (2008) 501–510, http://dx.doi.org/10.1016/j.carbon.2007.12.016.
[13] C. Hu, S. Sedghi, A. Silvestre-Albero, G.G. Andersson, A. Sharma, P. Pendleton, F. Rodríguez-Reinoso, K. Kaneko, M.J. Biggs, Raman spectroscopy study of the transformation of the carbonaceous skeleton of a polymer-based nanoporous carbon along the thermal annealing pathway, Carbon N. Y. 85 (2015) 147–158, http://dx.doi.org/10.1016/j.carbon.2014.12.098.
[14] K.W. McNamara, P. Ayyappan, R. Rajagopalan, J.G. Chen, H.C. Foley, Localized crystallization of polyfurfuryl alcohol derived carbon by alkali metals, Carbon N. Y. 56 (2013) 109–120, http://dx.doi.org/10.1016/j.carbon.2012.12.077.
[15] T. Hirasaki, T. Meguro, T. Wakihara, J. Tatami, K. Komeya, Glass-like carbon derived from a polymer consisting of furfuryl alcohol and tetraethylene glycol, J. Mater. Sci. 42 (2007) 7604–7606, http://dx.doi.org/10.1007/s10853-007-1890-5.
[16] L.A. Pesin, Review: structure and properties of glass-like carbon, J. Mater. Sci. 37 (2002) 1–28, http://dx.doi.org/10.1023/A:1013100920130.
[17] J. Kim, M.-S. Kim, H.-S. Hahm, Y.-S. Lim, Structural and property changes in glass-like carbons formed by heat treatment and addition of filler, Macromol. Res. 12 (2004) 399–406, http://dx.doi.org/10.1007/BF03218418.
[18] A. Gandini, M.N. Belgacem, Furans in polymer chemistry, Prog. Polym. Sci. 22 (1997) 1203–1379, http://dx.doi.org/10.1016/S0079-6700(97)00004-X.
[19] R. Gonzalez, J.M. Figueroa, H. Gonzalez, Furfuryl alcohol polymerization by iodine in methylene chloride, Eur. Polym. J. 38 (2001) 287–297.
[20] M. Principe, P. Ortiz, R. Martínez, An NMR study of poly(furfuryl alcohol) prepared with p-toluenesulphonic acid, Polym. Int. 48 (1999) 637–641 http://www.scopus.com/scopus/inward/record.url?eid=2-s2.0-0033176726&partnerID=40&rel=R7.0.0.
[21] L.-T. Cheng, W.J. Tseng, Effect of acid treatment on structure and morphology of carbons prepared from pyrolysis of polyfurfuryl alcohol, J. Polym. Res. 17 (2010) 391–399, http://dx.doi.org/10.1007/s10965-009-9325-4.
[22] M. Principe, R. Martínez, P. Ortiz, J. Rieumont, The polymerization of furfuryl alcohol with p-toluenesulfonic acid: photocross-linkeable feature of the polymer, Polímeros 10 (2000) 08–14, http://dx.doi.org/10.1590/S0104-14282000000100004.
[23] A.J. Jacobsen, S. Mahoney, W.B. Carter, S. Nutt, Vitreous carbon micro-lattice structures, Carbon N. Y. 49 (2011) 1025–1032, http://dx.doi.org/10.1016/j.carbon.2010.10.059.
[24] A. Dekanski, J. Stevanović, R. Stevanović, B.Ž. Nikolić, V.M. Jovanović, Glassy carbon electrodes, Carbon N. Y. 39 (2001) 1195–1205, http://dx.doi.org/10.1016/S0008-6223(00)00228-1.
[25] J.M. Friedrich, C. Ponce-de-León, G.W. Reade, F.C. Walsh, Reticulated vitreous carbon as an electrode material, J. Electroanal. Chem. 561 (2004) 203–217, http://dx.doi.org/10.1016/j.jelechem.2003.07.019.
[26] M.I. Awad, M.M. Saleh, T. Ohsaka, Recent progress in the electrochemistry of planar and reticulated vitreous carbon: fundamentals and applications, Curr. Top. Electrochem. 17 (2012) 15–40.
[27] M. Inagaki, J. Qiu, Q. Guo, Carbon foam: preparation and application, Carbon N. Y. 87 (2015) 128–152, http://dx.doi.org/10.1016/j.carbon.2015.02.021.
[28] A. Ōya, S. Ōtani, Catalytic graphitization of carbons by various metals, Carbon N. Y. 17 (1979) 131–137, http://dx.doi.org/10.1016/0008-6223(79)90020-4.
[29] A. Oya, S. Otani, Influences of particle size of metal on catalytic graphitization of non-graphitizing carbons, Carbon N. Y. 19 (1981) 391–400, http://dx.doi.org/10.1016/0008-6223(81)90064-6.
[30] W. Weisweiler, N. Subramanian, B. Terwiesch, Catalytic influence of metal melts on the graphitization of monolithic glasslike carbon, Carbon N. Y. 9 (1971) 755–761, http://dx.doi.org/10.1016/0008-6223(71)90008-X.
[31] M. Nakamizo, Raman spectra of iron-containing glassy carbons, Carbon N. Y. 29 (1991) 757–761, http://dx.doi.org/10.1016/0008-6223(91)90014-A.
[32] M.J. Bleda-Martínez, D. Lozano-Castelló, E. Morallón, D. Cazorla-Amorós, A. Linares-Solano, Chemical and electrochemical characterization of porous carbon materials, Carbon N. Y. 44 (2006) 2642–2651, http://dx.doi.org/10.1016/j.carbon.2006.04.017.
[33] H.P. Boehm, Surface oxides on carbon and their analysis: a critical assessment, Carbon N. Y. 40 (2002) 145–149, http://dx.doi.org/10.1016/S0008-6223(01)00165-8.
[34] J. Collins, D. Zheng, T. Ngo, D. Qu, M. Foster, Partial graphitization of activated carbon by surface acidification, Carbon N. Y. 79 (2014) 500–517, http://dx.doi.org/10.1016/j.carbon.2014.08.009.
[35] S.S. Oishi, M.C. Rezende, F.D. Origo, A.J. Damião, E.C. Botelho, Viscosity, pH, and moisture effect in the porosity of poly(furfuryl alcohol), J.Appl. Polym. Sci. 128 (2013) 1680–1686, http://dx.doi.org/10.1002/app.38332.
[36] A. Amiri, M. Shanbedi, G. Ahmadi, H. Eshghi, S.N. Kazi, B.T. Chew, Mass production of highly-porous graphene for high-performance supercapacitors, Nat. Publ. Gr. (2016) 1–11, http://dx.doi.org/10.1038/srep32686.
[37] N. Guigo, A. Mija, L. Vincent, N. Sbirrazzuoli, Chemorheological analysis and model-free kinetics of acid catalysed furfuryl alcohol polymerization, Phys. Chem. Chem. Phys. 9 (2007) 5359–5366, http://dx.doi.org/10.1039/b707950h.
[38] S. Bertarione, F. Bonino, F. Cesano, S. Jain, M. Zanetti, D. Scarano, A. Zecchina, Micro-FTIR and micro-raman studies of a carbon film prepared from furfuryl alcohol polymerization, J. Phys. Chem. B. 113 (2009) 10571–10574, http://dx.doi.org/10.1021/jp9050534.
[39] M. Choura, N.M. Belgacem, A. Gandini, Acid-catalyzed polycondensation of furfuryl alcohol: mechanisms of chromophore formation and cross-linking, Macromolecules 29 (1996) 3839–3850, http://dx.doi.org/10.1021/ma951522f.
[40] S. Barsberg, L.G. Thygesen, Poly(furfuryl alcohol) formation in neat furfuryl alcohol and in cymene studied by ATR-IR spectroscopy and density functional theory (B3LYP) prediction of vibrational bands, Vib. Spectrosc. 49 (2009) 52–63, http://dx.doi.org/10.1016/j.vibspec.2008.04.013.
[41] Y.-Q. Wang, H. Viswanathan, A.A. Audi, P.M.A. Sherwood, X-ray photoelectron spectroscopic studies of carbon fiber surfaces. 22. comparison between surface treatment of untreated and previously surface-treated fibers, Chem. Mater. 12 (2000) 1100–1107, http://dx.doi.org/10.1021/cm990734e.
[42] N. Suzuki, Chapter 13 – X-ray photoelectron spectroscopy and its application to carbon, Carbon Alloy (2003) 211–222, http://dx.doi.org/10.1016/B978-008044163-4/50013-9.
[43] P.M.A. Sherwood, Surface analysis of carbon and carbon fibers for composites, J. Electron Spectrosc. Relat. Phenom. 81 (1996) 319–342, http://dx.doi.org/10.1016/0368-2048(95)02529-4.
[44] S. Yumitori, Correlation of C1s chemical state intensities with the O1s intensity in the XPS analysis of anodically oxidized glass-like carbon samples, J. Mater. Sci. 35 (2000) 139–146, http://dx.doi.org/10.1023/A:1004761103919.
[45] C.U. Pittman, W. Jiang, Z.R. Yue, S. Gardner, L. Wang, H. Toghiani, C. a. Leon Y Leon, Surface properties of electrochemically oxidized carbon fibers, Carbon N. Y. 37 (1999) 1797–1807, http://dx.doi.org/10.1016/S0008-6223(99)00048-2.
[46] C.L. Weitzsacker, M. Xie, L.T. Drzal, Using XPS to investigate fiber/matrix chemical interactions in carbon-fiber-reinforced composites, Surf. Interface

Anal. 25 (1997) 53–63, http://dx.doi.org/10.1002/(SICI)1096-9918(199702)25:2<53:AID-SIA222>3.0.CO;2-E.
[47] C.-W. Huang, H.-C. Wu, W.-H. Lin, Y.-Y. Li, Temperature effect on the formation of catalysts for growth of carbon nanofibers, Carbon N. Y. 47 (2009) 795–803, http://dx.doi.org/10.1016/j.carbon.2008.11.033.
[48] A. Perrard, L. Retailleau, R. Berjoan, J.P. Joly, Liquid phase oxidation kinetics of an ex-cellulose activated carbon cloth by NaOCl, Carbon N. Y. 50 (2012) 2226–2234, http://dx.doi.org/10.1016/j.carbon.2012.01.039.
[49] J. Figueiredo, M.F. Pereira, M.M. Freitas, J.J. Órfão, Modification of the surface chemistry of activated carbons, Carbon N. Y. 37 (1999) 1379–1389, http://dx.doi.org/10.1016/S0008-6223(98)00333-9.
[50] J.L. Figueiredo, M.F.R. Pereira, The role of surface chemistry in catalysis with carbons, Catal. Today 150 (2010) 2–7, http://dx.doi.org/10.1016/j.cattod.2009.04.010.
[51] Y.-J. Lee, The second order Raman spectroscopy in carbon crystallinity, J. Nucl. Mater. 325 (2004) 174–179, http://dx.doi.org/10.1016/j.jnucmat.2003.12.005.
[52] L. Lu, V. Sahajwalla, C. Kong, D. Harris, Quantitative X-ray diffraction analysis and its application to various coals, Carbon N. Y. 39 (2001) 1821, http://dx.doi.org/10.1016/s0008-6223(00)00318-3.
[53] A. Cuesta, P. Dhamelincourt, J. Laureyns, A. Martinez-Alonso, J.M.D. Tascon, Comparative performance of X-ray diffraction and Raman microprobe techniques for the study of carbon materials, J. Mater. Chem. 8 (1998) 2875–2879, http://dx.doi.org/10.1039/A805841E.
[54] M.R. Baldan, E.C. Almeida, A.F. Azevedo, E.S. Gonçalves, M.C. Rezende, N.G. Ferreira, Raman validity for crystallite size La determination on reticulated vitreous carbon with different graphitization index, Appl. Surf. Sci. 254 (2007) 600–603, http://dx.doi.org/10.1016/j.apsusc.2007.06.038.
[55] a. Ferrari, J. Robertson, Interpretation of Raman spectra of disordered and amorphous carbon, Phys. Rev. B 61 (2000) 14095–14107, http://dx.doi.org/10.1103/PhysRevB.61.14095.
[56] T. Jawhari, A. Roid, J. Casado, Raman spectroscopic characterization of some commercially available carbon black materials, Carbon N. Y. 33 (1995) 1561–1565, http://dx.doi.org/10.1016/0008-6223(95)00117-V.
[57] K. Takai, M. Oga, H. Sato, T. Enoki, Y. Ohki, A. Taomoto, K. Suenaga, S. Iijima, Structure and electronic properties of a nongraphitic disordered carbon system and its heat-treatment effects, Phys. Rev. B 67 (2003) 1–11, http://dx.doi.org/10.1103/PhysRevB.67.214202.
[58] T.-H. Ko, W.-S. Kuo, Y.-H. Chang, Raman study of the microstructure changes of phenolic resin during pyrolysis, Polym. Compos. 21 (2000) 745–750, http://dx.doi.org/10.1002/pc.10229.
[59] A. Sadezky, H. Muckenhuber, H. Grothe, R. Niessner, U. Pöschl, Raman microspectroscopy of soot and related carbonaceous materials: spectral analysis and structural information, Carbon N. Y. 43 (2005) 1731–1742, http://dx.doi.org/10.1016/j.carbon.2005.02.018.
[60] S. Vollebregt, R. Ishihara, F.D. Tichelaar, Y. Hou, C.I.M. Beenakker, Influence of the growth temperature on the first and second-order Raman band ratios and widths of carbon nanotubes and fibers, Carbon N. Y. 50 (2012) 3542–3554, http://dx.doi.org/10.1016/j.carbon.2012.03.026.
[61] P. Mallet-Ladeira, P. Puech, C. Toulouse, M. Cazayous, N. Ratel-Ramond, P. Weisbecker, G.L. Vignoles, M. Monthioux, A Raman study to obtain crystallite size of carbon materials: a better alternative to the Tuinstra–Koenig law, Carbon N. Y. 80 (2014) 629–639, http://dx.doi.org/10.1016/j.carbon.2014.09.006.
[62] E.B. Barros, A.G. Souza Filho, H. Son, M.S. Dresselhaus, G??? band raman lineshape analysis in graphitic foams, Vib. Spectrosc. 45 (2007) 122–127, http://dx.doi.org/10.1016/j.vibspec.2007.08.002.
[63] B.A. Samuel, R. Rajagopalan, H.C. Foley, M.A. Haque, Effect of pyrolysis temperature on the microstructure of disordered carbon nanowires, Thin Solid Films 519 (2010) 91–95, http://dx.doi.org/10.1016/j.tsf.2010.07.066.
[64] S.S. Bukalov, L. a Leites, a I. Sorokin, a S. Kotosonov, Structural changes in industrial glassy carbon as a function of heat treatment temperature according to raman spectroscopy and X-Ray, Nanosyst. Physics Chem. Math. 5 (2014) 186–191.
[65] E.S. Goncalves, M.C. Rezende, N.G. Ferreira, Dynamics of defects and surface structure formation in reticulated vitreous carbon, Braz. J. Phys. 36 (2006) 264–266, http://dx.doi.org/10.1590/S0103-97332006000300008.
[66] G. Li, Z. Lu, B. Huang, Z. Wang, H. Huang, R. Xue, L. Chen, Raman scattering investigation of carbons obtained by heat treatment of a polyfurfuryl alcohol, Solid State Ion. 89 (1996) 327–331, http://dx.doi.org/10.1016/0167-2738(96)00352-9.
[67] Y.-S. Lim, H.-S. Kim, M.-S. Kim, N.-H. Cho, S. Nahm, Chemical and micro-structural changes in glass-like carbon during high temperature heat treatment, Macromol. Res. 11 (2003) 122–127, http://dx.doi.org/10.1007/BF03218341.
[68] E.F. Antunes, A.O. Lobo, E.J. Corat, V.J. Trava-Airoldi, Influence of diameter in the Raman spectra of aligned multi-walled carbon nanotubes, Carbon N.Y. 45 (2007) 913–921, http://dx.doi.org/10.1016/j.carbon.2007.01.003.
[69] E.B. Barros, N.S. Demir, A.G. Souza Filho, J. Mendes Filho, A. Jorio, G. Dresselhaus, M.S. Dresselhaus, Raman spectroscopy of graphitic foams, Phys. Rev. B: Condens. Matter Mater. Phys. 71 (2005) 1–5, http://dx.doi.org/10.1103/PhysRevB.71.165422.
[70] L.G. Caņado, K. Takai, T. Enoki, M. Endo, Y.A. Kim, H. Mizusaki, A. Jorio, L.N. Coelho, R. Magalhães-Paniago, M.A. Pimenta, General equation for the determination of the crystallite size la of nanographite by Raman spectroscopy, Appl. Phys. Lett. 88 (2006) 12–14, http://dx.doi.org/10.1063/1.2196057.
[71] H.K. Arzani, A. Amiri, S.N. Kazi, A. Badarudin, B.T. Chew, RSC Advances tetrahydrofurfuryl polyethylene glycol-treated, RSC Adv. 6 (2016) 65654–65669, http://dx.doi.org/10.1039/C6RA13301K.
[72] H.C. Foley, Carbogenic molecular sieves: synthesis, properties and applications, Microporous Mater. 4 (1995) 407–433.
[73] J. Collins, T. Ngo, D. Qu, M. Foster, Spectroscopic investigations of sequential nitric acid treatments on granulated activated carbon: effects of surface oxygen groups on π density, Carbon N. Y. 57 (2013) 174–183, http://dx.doi.org/10.1016/j.carbon.2013.01.061.